The Japan Society
of Applied Physics

REGULAR PAPER

Design and measurement of broadband loop mirror with curved directional coupler based on Si waveguides

View the article online for updates and enhancements.

REGULAR PAPER

Design and measurement of broadband loop mirror with curved directional coupler based on Si waveguides

Takuya Mitarai[1], Eissa Moataz[1], Takayuki Miyazaki[1], Tomohiro Amemiya[1,2], and Nobuhiko Nishiyama[1,2*]

[1]Department of Electrical and Electronic Engineering, Tokyo Institute of Technology, O-okayama, Meguro, Tokyo 152-8552, Japan
[2]Institute of Innovative Research (IIR), Tokyo Institute of Technology, O-okayama, Meguro, Tokyo 152-8552, Japan

*E-mail: nishiyama@ee.e.titech.ac.jp

Toward the realization of an external cavity type III–V/SOI hybrid tunable laser with wavelength-insensitive operation, a broadband silicon waveguide loop mirror with a curved directional coupler (CDC) was developed, and flat reflectance spectra were demonstrated. Flat reflectance was obtained in the entire C band using the CDC. Reflectance was changed from 16% to 95% by varying the coupling angle of the CDC. The standard deviation of the reflectance of the loop mirror with the straight directional coupler was 5.9 points in the C band, while that for the loop mirror with the CDC was 1.9 points. © 2020 The Japan Society of Applied Physics

1. Introduction

A large number of optical channels are installed in wavelength division multiplexing photonic networks to handle rapidly increasing data traffic.[1] Therefore, silicon (Si)-based photonic integrated circuits (PICs), which can operate in a broadband wavelength range, are used as optical communication devices.[2–4] The III–V/SOI hybrid tunable laser has been studied[5–8] as an integrated tunable laser source in Si-based PICs. The III–V/SOI hybrid tunable laser should exhibit the following properties: single-mode operation with a narrow linewidth, stable tunability, and high efficiency in the entire operation range. Previous studies have shown the improvement of the hybrid laser in various aspects, such as the optical coupling between the III–V structure and Si waveguide[9,10] and the III–V/SOI bonding process.[11–13] In particular, the cavity structure of the hybrid laser has been considered as, for example, the microdisk of the III–V active layer type,[14,15] distributed Bragg reflector (DBR) type,[16,17] distributed feedback type,[18–23] external ring reflector type,[13,24] or cavity on external chip type.[25–27] According to the laser theory, we must consider two components of lasers, i.e. a mirror and the optical gain in an active region, to realize stable operation (and ultimately wavelength-insensitive power and linewidth) in the entire operation range. In this work, we focus on the mirror component of a cavity created using Si waveguides.

Uniform (wavelength insensitive) mirror loss (or reflectance) is required to achieve lasing characteristics in the entire tuning range of hybrid tunable lasers. Even though lasing characteristics are determined by both mirror loss and optical gain characteristics in the laser theory, the characteristics of conventional tunable in-plane lasers in the InP system are limited by mirror characteristics.[28] A loop mirror can be used to solve this problem in Si photonics.[29] However, the reflectance of a loop mirror is determined by the characteristics of a directional coupler, which typically depend on wavelength. A curved directional coupler (CDC) has been proposed for achieving wavelength-insensitive characteristics. The CDC can reduce the wavelength dependence of the directional coupler designed with curved waveguides.[30–32] Unlike another type of asymmetric directional coupler such as one with waveguides that have asymmetric width, the CDC does not require the precise

control of the structure for broadband operation. We used the CDC structure and demonstrated the preliminary results of a broadband loop mirror.[33] In this paper, we present the detailed design, fabrication, and improved measurement results of a broadband loop mirror that utilizes a CDC. The rest of this paper is organized as follows: the operating principle and actual design of the loop mirror are explained in Sects. 2 and 3, respectively. The fabrication and measurement results are described in Sect. 4. The conclusions are provided in Sect. 5.

2. Operating principle

The proposed loop mirror consists of a CDC and a loop waveguide, as shown in Fig. 1. The reflectance of the loop mirror strongly depends on the characteristics of the coupler. Therefore, it is necessary to reduce the wavelength dependence of the coupler to realize a broadband loop mirror. As shown in Fig. 2, the power splitting ratio at the bar port (P_{bar}) of a conventional directional coupler, which is created using straight and symmetric waveguides, varies sinusoidally from 0 to 1 based on wavelength. In a high reflectance loop mirror, the coupler must have $P_{\mathrm{bar}} \sim 0.5$ (the region indicated by "Inclined"). The power ratio of a conventional coupler strongly depends on wavelength. In contrast, in an asymmetric coupler with bent waveguides, the dependence of P_{bar} on wavelength is limited by the detuning parameters between waveguides. The wavelength dependence of the P_{bar} of a coupler can be reduced in the flat region. This decreases the wavelength dependence of a loop mirror.

3. Design and simulation result

In our experiments, these devices, the coupler, and the loop mirror were designed for TE-mode light because it was assumed to be applied to a gain medium for the TE mode and operated in the C band (1530–1565 nm) toward a tunable laser. Figure 3 shows the schematic of the cross-section of the coupler, which contains Si wire waveguides with thicknesses of 235 and 500 nm. The gap width is 200 nm. To avoid a problem at bonding in the fabrication process of hybrid lasers, we intentionally adopted a rib waveguide structure with 40 nm thick Si for the exterior of the waveguide. In the gap, there was 90 nm thick Si owing to the microloading effect in dry etching on the waveguide formation process. Of course, full mesa etching can be used for such as silicon
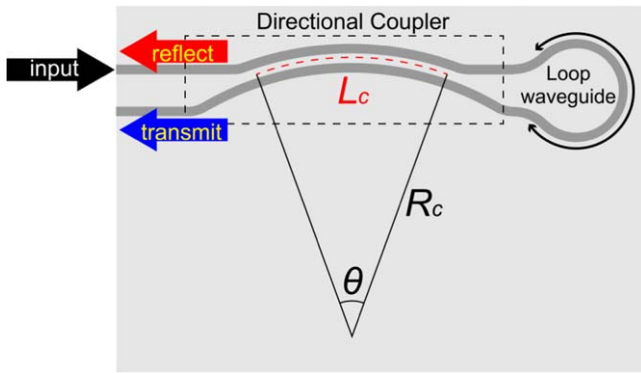
© 2020 The Japan Society of Applied Physics

Fig. 1.   (Color online) Schematic of the loop mirror with the CDC.

Fig. 3.   (Color online) Schematic of the cross-section of the coupler.

monolithic photonic circuit if required. As shown in Fig. 1, the CDC has three design parameters: the coupler length, L_c, the coupling angle, θ, and the bending angle, R_c. L_c was set to obtain the desired operation wavelength, and θ was set to obtain a desired power splitting ratio. R_c was derived from the ratio of L_c and θ. 3D-finite-difference time-domain software was used for the design and simulation of the coupler.

First, L_c should be the same as the beat length of a straight coupler with the same cross-sectional waveguide structures as shown in Fig. 3 at a target center wavelength, λ_c, which is 1550 nm for C-band operation. Figure 4 shows the relationship between the power splitting ratio at the bar port (P_{bar}) of the straight coupler and the coupler length obtained through simulation. The model of the simulation is also shown in the inset of Fig. 4. In the simulation, the weak coupling between approaching waveguides was also considered. Therefore, $P_{bar} = 1$ could not be obtained even at $L_c = 0$ or 25 μm. L_c at the minimum P_{bar} was estimated to be 12 μm. Next, to realize an arbitrary P_{bar}, L_c was fixed and θ was varied from 10° to 35° to show that P_{bar} changed with θ. The result is shown in Fig. 5(a). Every CDC shows flat wavelength characteristics of P_{bar} in the entire C-band and various P_{bar} corresponding to θ could be obtained. It can be seen that couplers with large θ tend to have small P_{bar} (i.e. weak coupling). $P_{bar} = 0.5$, namely 3 dB coupler can be obtained at $\theta = 20°$. In Fig. 5(b), wavelength characteristics of the straight coupler with 5 μm length, and the CDC with $\theta = 20°$ are compared. It is clear that the fluctuation of P_{bar} was suppressed in a CDC compared with a straight coupler. P_{bar} of this CDC varies 0.5 points (from 46.9% to 47.4%),
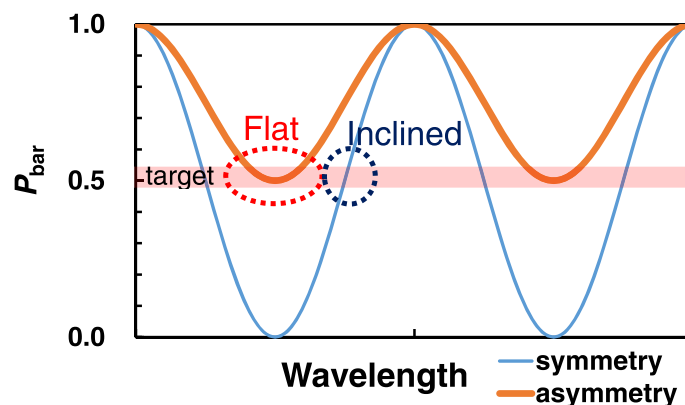
whereas P_{bar} of this straight coupler varies 7.2 points (from 47.3% to 54.6%) in C-band. Even in the range of much wider band such as including S and L-band, better characteristics can be observed compared with the conventional straight coupler.

In the loop mirror structure as shown in Fig. 1, the input light is divided by the coupler, and both lights from the bar and cross port pass through the loop waveguide independently. Then, they interact in the coupler, and two lights that are reflected and transmitted are taken out. In this way, input light passed through the coupler twice, so that Eq. (1) was used to calculate the characteristics of the loop mirror with the coupler. The reflectance and transmittance of the loop mirror were derived by operating the propagation matrix of the coupler twice. In this equation, t indicates the transmission coefficient of the electric field, which can be obtained from the square root of P_{bar}. κ indicates the coupling coefficient of the electric field, which is obtained as the sum of the magnitudes of t and κ. For example, a mirror with a 30% reflectance requires a coupler with $P_{bar} = 0.92$ or 0.08. However, $P_{bar} = 0.92$ may be preferable in terms of better wavelength dependence. For much higher reflectance of over 99%, P_{bar} with the range of 0.45–0.55 can be applied and the reflectance reaches a maximum at the P_{bar} of 0.5.

The reflectance for each θ is calculated using Eq. (1) and shown in Fig. 5(c)

Fig. 2.   (Color online) Comparison of spectra of P_{bar} between the symmetric coupler and asymmetric coupler.

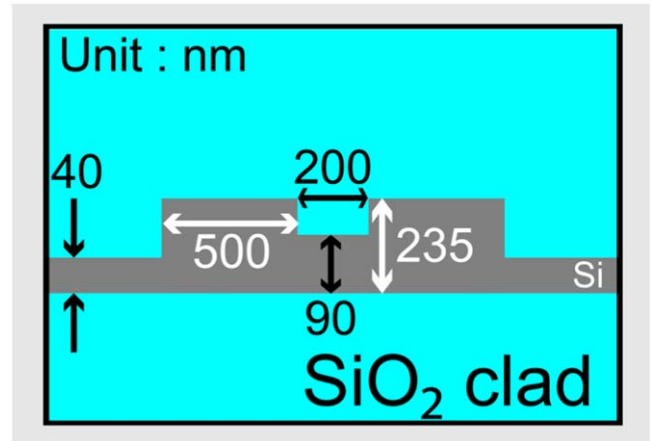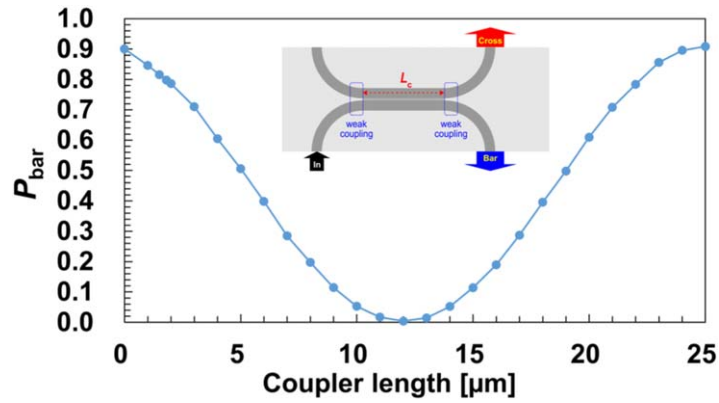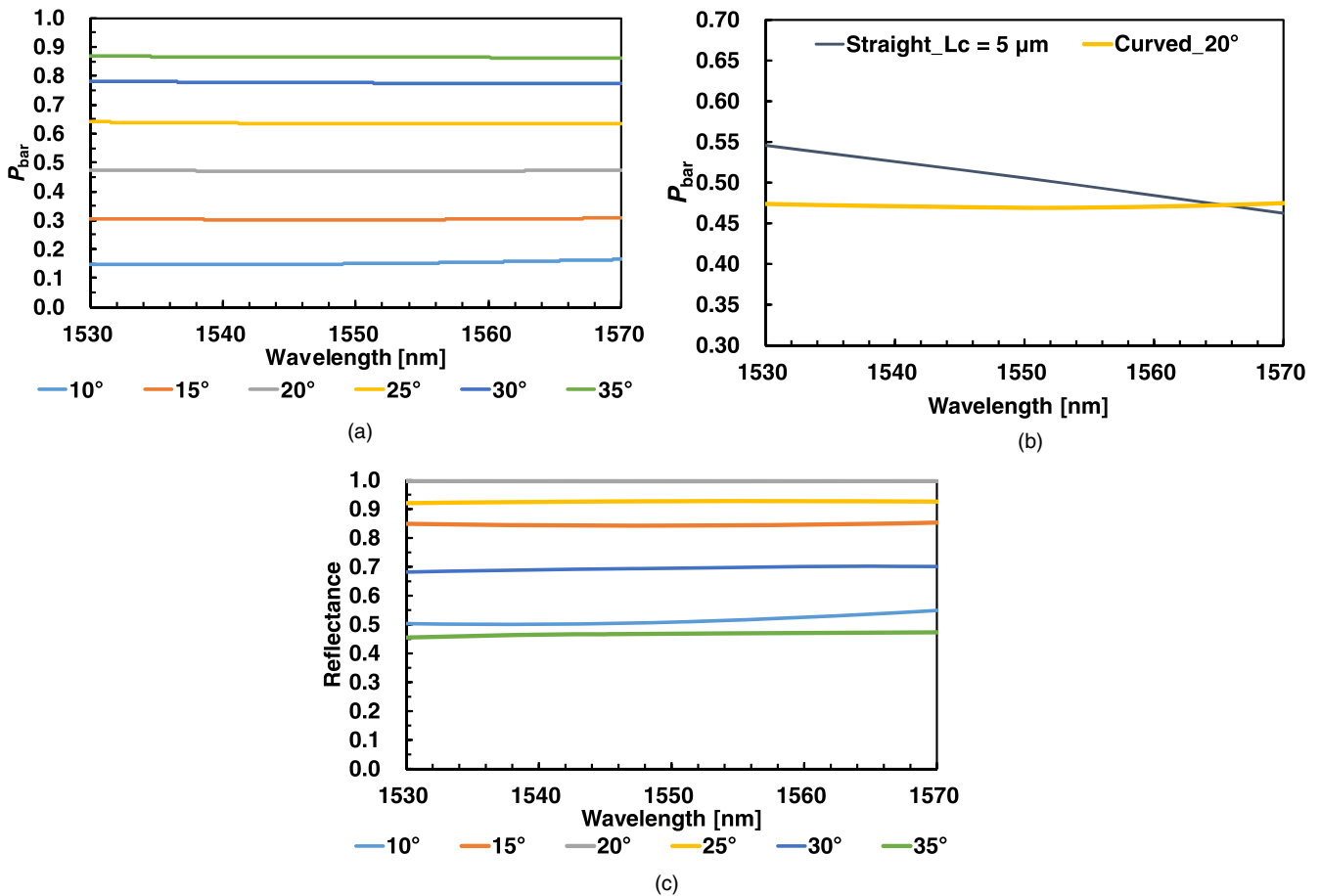**Fig. 4.** (Color online) P_{bar} of the straight coupler with respect to coupler length.

Fig. 5. (Color online) (a) Simulated P_{bar} of the CDC at various angles. (b) Comparison of wavelength dependency between the CDC and the straight coupler. (c) Simulated reflectance of the loop mirror at various angles.

$$\begin{pmatrix} \text{Reflectance} \\ \text{Transmittance} \end{pmatrix} = \begin{pmatrix} t & j\kappa \\ j\kappa^* & t^* \end{pmatrix} \begin{pmatrix} t & j\kappa \\ j\kappa^* & t^* \end{pmatrix} \begin{pmatrix} \text{Input} \\ 0 \end{pmatrix}$$

$$= \begin{pmatrix} 4P_{bar}(1 - P_{bar}) \\ (2P_{bar} - 1)^2 \end{pmatrix}. \qquad (1)$$

4. Fabrication and measurement

The loop mirror with the CDC was realized using a single etching process, unlike the top-grating DBR. As they were composed of only waveguides, the fabrication process was the same as that of waveguide circuits. The waveguides were fabricated by utilizing electron-beam lithography for forming waveguide circuit pattern and inductively-coupled-plasma reactive ion etching with a CF_4/SF_6 gas mixture for etching an SOI chip. Facets were exposed by breaking supported by partial dicing. Finally, the SiO_2 cladding layer was deposited using plasma-enhanced chemical vapor deposition. No additional antireflection coating was carried out. Figures 6(a) and 6(b) show a microscopic image of the entire device and a cross-sectional SEM image of the fabricated coupler, respectively.

Figure 7 shows the measurement systems for the CDC and loop mirror. The light from an amplified spontaneous emission light source was polarized to the TE mode through a polarizer. Then, the light was injected into the Si waveguide
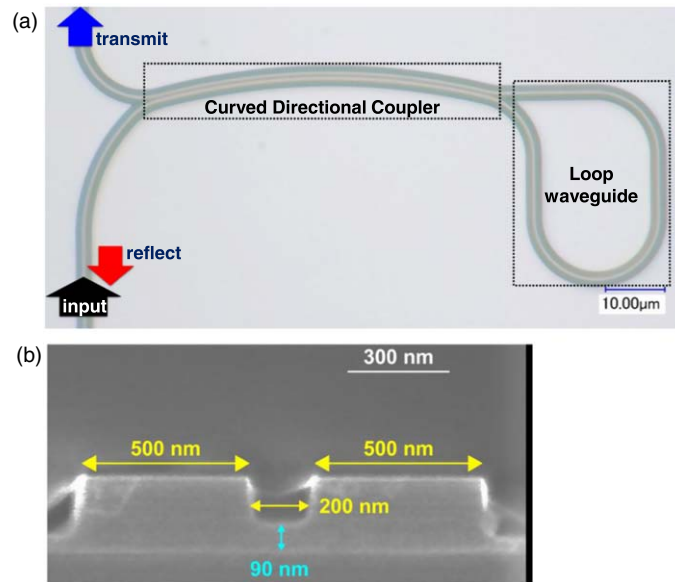
Fig. 6. (Color online) (a) Optical microscopic image of fabricated loop mirror. (b) SEM image of the cross-section of the coupler.
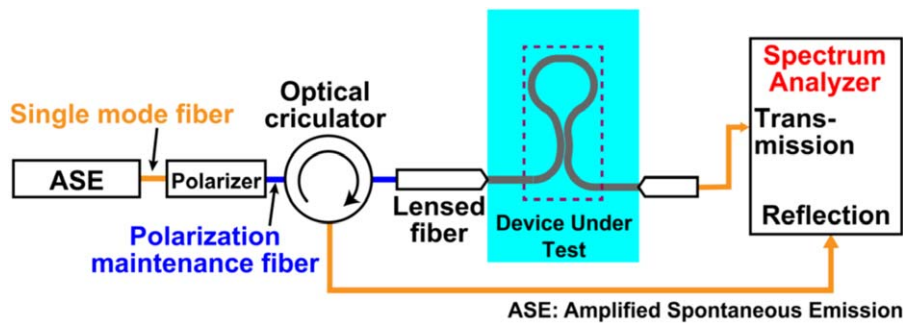

Fig. 7. (Color online) Measurement system for the coupler and loop mirror.

via a lensed fiber after it passed through an optical circulator. The reflected light was guided to a spectrum analyzer by the function of the circulator. In addition, transmitted light propagated to the other facet, where it was coupled to another lensed fiber to be measured by the spectrum analyzer.

In the coupler, P_{bar} was derived through four times measurement. We removed all losses using the measurement system shown in Fig. 8 and Eq. (2). Therefore, insertion loss could not be measured using this method. The reflectance of the loop mirror was calculated from the ratio of the reflected power and the sum of the reflected and transmitted powers, as given by Eq. (3).

Here, the insertion loss of the loop mirror was not considered under the assumption that the losses for reflection and transmission were same and facet reflection was neglected because it was relatively small

$$P_{bar} = \sqrt{\frac{T_1 T_2}{K_1 K_2}} \bigg/ \left(1 + \sqrt{\frac{T_1 T_2}{K_1 K_2}} \right). \quad (2)$$

$$\text{Reflectivity} = \frac{\text{Reflection}}{\text{Transmission} + \text{Reflection}}. \quad (3)$$

The relationship between the P_{bar} measured at 1550 nm and the length of the straight coupler is shown in Fig. 9. A cosine curve was obtained. The beat length was estimated to be 12 μm, which was in agreement with the simulation results.

Figure 10 shows the measured spectra of P_{bar} at various θ. Various values of P_{bar} were obtained with flat spectra. The differences between the simulation and measurement results
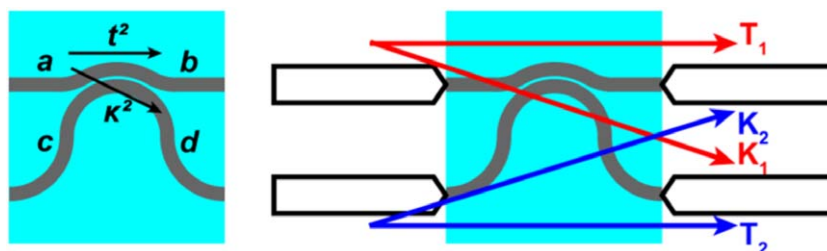

Fig. 8. (Color online) Measurement method to derive the characteristics of the coupler.
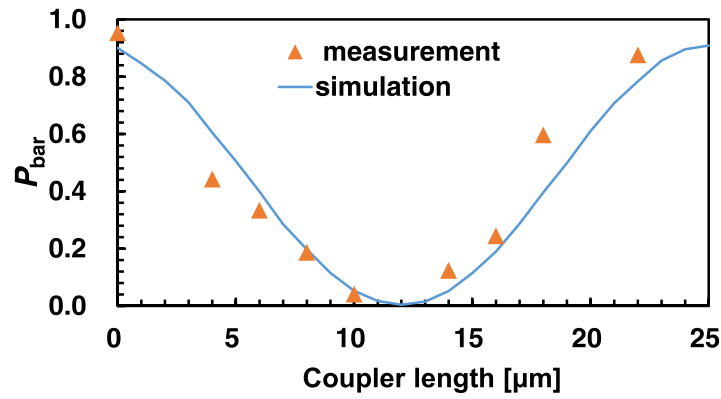
Fig. 9.   (Color online) Measured P_{bar} of the straight coupler at various lengths.
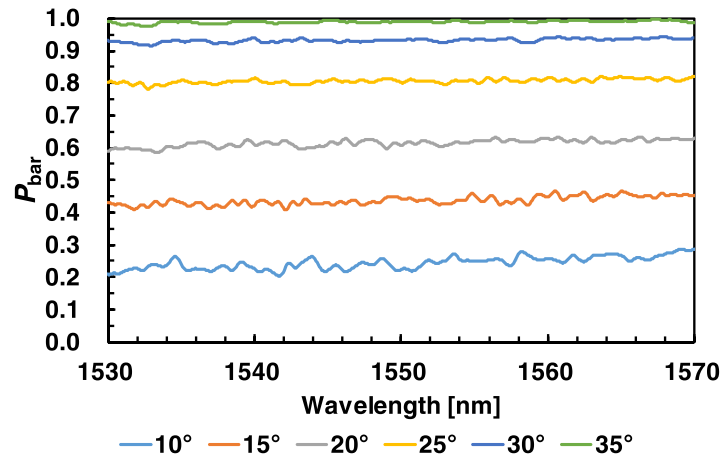

Fig. 10.   (Color online) Measured P_{bar} of the CDC at various angles.

were due to insertion loss, which was assumed to be caused by scattering at the coupler.

Figure 11 shows the measured spectra of the reflectance of the fabricated loop mirror with the CDC at various θ. Various values of reflectance were obtained with flat spectra. In addition, the loop mirror exhibited stronger wavelength dependence as θ decreased. The standard deviation of the reflectance of the loop mirror that used the CDC with $\theta = 10°$ and $25°$ was 4.6 points and 2.0 points, respectively. Based on the flat reflectance spectra, $\theta > 15°$ should be used for the loop mirror because the coupler with small θ showed slightly stronger wavelength dependence compared to the coupler with large θ. Reflectance was varied from 16% to 95% by changing θ. It is estimated that the difference from the simulation results shown in Fig. 5(c) was due to the mismatch between the simulation and measurement of the coupler and the reflection on the facet of the waveguide. As mentioned before, the loss was ignored in the measurement of the coupler but the simulation was not.

The comparison of the loop mirror with a conventional straight directional coupler and the loop mirror with the CDC is shown in Fig. 12. Flatter reflectance spectra were obtained
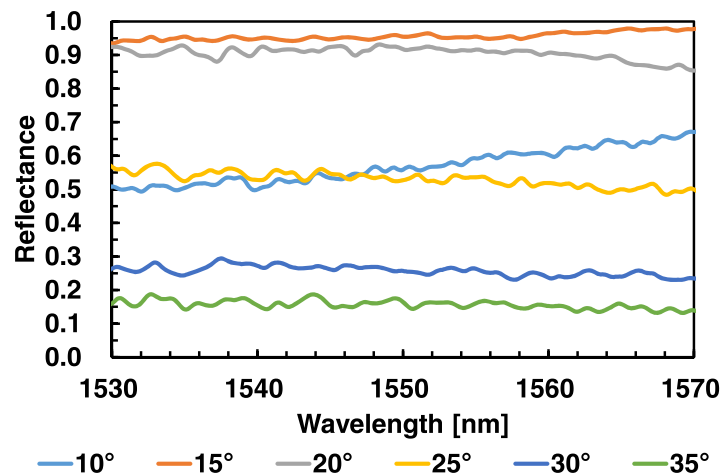

Fig. 11.   (Color online) Measured reflectance of the loop mirror with the CDC at various angles.
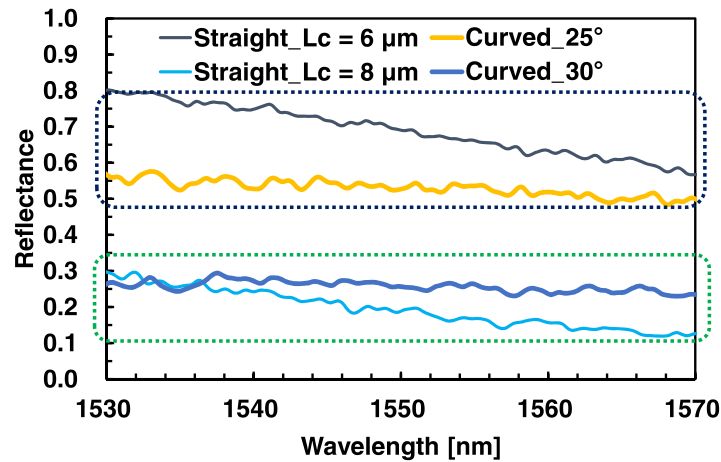
Fig. 12. (Color online) Comparison of the loop mirrors with the straight coupler and CDC.

for the loop mirror with the CDC. The standard deviation of the reflectance of the loop mirror that used the CDC with $\theta = 25°$ was 1.9 points, while that of the loop mirror that used the straight coupler with a length of 6 μm was 5.9 points.

5. Conclusion

A loop mirror with a CDC was fabricated to obtain flat reflectance spectra in the entire C-band. The reflectance of the loop mirror was changed from 16% to 95% by varying the coupling angle of the CDC. The standard deviation of the reflectance of the loop mirror with the CDC was 1.9 points in the C band, while that of the loop mirror with the conventional straight directional coupler was 5.9 points. This loop mirror with CDC can be a key element of broadband hybrid tunable lasers. Also, this low wavelength dependence means low-temperature dependence at a fixed wavelength. Such function gives robustness for future large scale PIC on a Si-platform.

ORCID iDs

Nobuhiko Nishiyama ⓘ https://orcid.org/0000-0001-8288-6690

1) CISCO, Cisco Visual Networking Index: Global Mobile Data Traffic Forecast Update, 2017–2022 (2019).
2) R. Soref, IEEE J. Sel. Top. Quantum Electron. **12**, 1678 (2006).
3) P. Dong, X. Liu, S. Chandrasekhar, L. L. Buhl, R. Aroca, and Y. K. Chen, IEEE J. Sel. Top. Quantum Electron. **20**, 6100108 (2014).
4) D. Thomson et al., J. Opt. **18**, 073003 (2016).
5) A. W. Fang, H. Park, O. Cohen, R. Jones, M. J. Paniccia, and J. E. Bowers, Opt. Express **14**, 9203 (2006).
6) A. W. Fang, R. Jones, H. Park, O. Cohen, O. Raday, M. J. Paniccia, and J. E. Bowers, Opt. Express **15**, 2315 (2007).
7) X. Sun, A. Zadok, M. J. Shearn, K. A. Diest, A. Ghaffari, H. A. Atwater, A. Scherer, and A. Yariv, Opt. Lett. **34**, 1345 (2009).
8) B. Song, C. Stagarescu, S. Ristic, A. Behfar, and J. Klamkin, Opt. Express **24**, 10435 (2016).
9) J. Suzuki, F. Tachibana, K. Nagasaka, M. S. A. M. Eissa, L. Bai, T. Mitarai, T. Amemiya, N. Nishiyama, and S. Arai, Jpn. J. Appl. Phys. **57**, 094101 (2018).
10) B. Ben Bakir, A. Descos, N. Olivier, D. Bordel, P. Grosse, E. Augendre, L. Fulbert, and J. M. Fedeli, Opt. Express **19**, 10317 (2011).
11) D. Liang, J. E. Bowers, D. C. Oakley, A. Napoleone, D. C. Chapman, C.-L. Chen, P. W. Juodawlkis, and O. Raday, Electrochem. Solid-State Lett. **12**, H101 (2009).
12) S. Stanković, R. Jones, M. N. Sysak, J. M. Heck, G. Roelkens, and D. Van Thourhout, IEEE Photonics Technol. Lett. **23**, 1781 (2011).
13) Y. Hayashi, J. Suzuki, S. Inoue, S. M. T. Hasan, Y. Kuno, K. Itoh, T. Amemiya, N. Nishiyama, and S. Arai, Jpn. J. Appl. Phys. **55**, 082701 (2016).
14) J. Van Campenhout, P. Rojo-Romeo, P. Regreny, C. Seassal, D. Van Thourhout, S. Verstuyft, L. Di Cioccio, J.-M. Fedeli, C. Lagahe, and R. Baets, Opt. Express **15**, 6744 (2007).
15) D. Liang, X. Huang, G. Kurczveil, M. Fiorentino, and R. G. Beausoleil, Nat. Photonics **10**, 719 (2016).
16) A. W. Fang, B. R. Koch, R. Jones, E. Lively, D. Liang, Y.-H. Kuo, and J. E. Bowers, IEEE Photonics Technol. Lett. **20**, 1667 (2008).
17) D. Huang, M. A. Tran, J. Guo, J. Peters, T. Komljenovic, A. Malik, P. A. Morton, and J. E. Bowers, Optica **6**, 745 (2019).
18) A. W. Fang, E. Lively, Y.-H. Kuo, D. Liang, and J. E. Bowers, Opt. Express **16**, 4413 (2008).
19) C. Zhang, S. Srinivasan, Y. Tang, M. J. R. Heck, M. L. Davenport, and J. E. Bowers, Opt. Express **22**, 10202 (2014).
20) Y.-L. Cao et al., Opt. Express **23**, 8800 (2015).
21) S. Dhoore, L. Li, A. Abbasi, G. Roelkens, and G. Morthier, IEEE Photonics Technol. Lett. **28**, 2343 (2016).
22) A. Abbasi et al., IEEE Photonics Technol. Lett. **30**, 1095 (2018).
23) S. Dhoore, A. Köninger, R. Meyer, G. Roelkens, and G. Morthier, Laser Photonics Rev. **13**, 1800287 (2019).
24) J. Zhang et al., APL Photonics **4**, 110803 (2019).
25) T. Kita, K. Nemoto, and H. Yamada, Jpn. J. Appl. Phys. **53**, 04EG04 (2014).
26) N. Kobayashi, K. Sato, M. Namiwaka, K. Yamamoto, S. Watanabe, T. Kita, H. Yamada, and H. Yamazaki, J. Lightwave Technol. **33**, 1241 (2015).
27) H. Guan et al., Opt. Express **26**, 7920 (2018).
28) H. Yagi, T. Kaneko, N. Kono, Y. Yoneda, K. Uesaka, M. Ekawa, M. Takechi, and H. Shoji, IEEE J. Sel. Top. Quantum Electron. **24**, 6100411 (2018).
29) Y. Zheng, D. Keh-Ting Ng, Y. Wei, W. Yadong, Y. Huang, Y. Tu, C.-W. Lee, B. Liu, and S.-T. Ho, Appl. Phys. Lett. **99**, 011103 (2011).
30) H. Morino, T. Maruyama, and K. Iiyama, J. Lightwave Technol. **32**, 2188 (2014).
31) S. Chen, Y. Shi, S. He, and D. Dai, Opt. Lett. **41**, 836 (2016).
32) G. F. R. Chen, J. R. Ong, T. Y. L. Ang, S. T. Lim, C. E. Png, and D. T. H. Tan, Sci. Rep. **7**, 7246 (2017).
33) T. Mitarai, M. Eissa, T. Miyazaki, T. Amemiya, N. Nishiyama, and S. Arai, 24th OECC/PSC, ME2-2, 2019, p. 1.